

## Dynamic and quantitative $\text{Ca}^{2+}$ measurements using improved cameleons

ATSUSHI MIYAWAKI\*<sup>†</sup>, OLIVER GRIESBECK\*<sup>‡</sup>, ROGER HEIM\*<sup>‡§</sup>, AND ROGER Y. TSJEN\*<sup>‡¶</sup>

\*Department of Pharmacology and the <sup>‡</sup>Howard Hughes Medical Institute, University of California, San Diego, La Jolla, CA 92093-0647

Contributed by Roger Y. Tsien, December 29, 1998

**ABSTRACT** Cameleons are genetically-encoded fluorescent indicators for  $\text{Ca}^{2+}$  based on green fluorescent protein variants and calmodulin (CaM). Because cameleons can be targeted genetically and imaged by one- or two-photon excitation microscopy, they offer great promise for monitoring  $\text{Ca}^{2+}$  in whole organisms, tissues, organelles, and submicroscopic environments in which measurements were previously impossible. However, the original cameleons suffered from significant pH interference, and their  $\text{Ca}^{2+}$ -buffering and cross-reactivity with endogenous CaM signaling pathways was uncharacterized. We have now greatly reduced the pH-sensitivity of the cameleons by introducing mutations V68L and Q69K into the acceptor yellow green fluorescent protein. The resulting new cameleons permit  $\text{Ca}^{2+}$  measurements despite significant cytosolic acidification. When  $\text{Ca}^{2+}$  is elevated, the CaM and CaM-binding peptide fused together in a cameleon predominantly interact with each other rather than with free CaM and CaM-dependent enzymes. Therefore, if cameleons are overexpressed, the primary effect is likely to be the unavoidable increase in  $\text{Ca}^{2+}$  buffering rather than specific perturbation of CaM-dependent signaling.

Cytosolic and organellar free  $\text{Ca}^{2+}$  concentrations show the most dramatic spatial and temporal fluctuations of any intracellular messenger.  $\text{Ca}^{2+}$  signals are most often measured by using synthetic fluorescent chelators (1) or the photoprotein aequorin (2). The chelators are easily imaged, but they are hard to target to specific intracellular locations, and they gradually leak out of cells, particularly at warmer temperatures. Loading of chelators via their acetoxyethyl esters is fairly noninvasive and easy in isolated cells from vertebrate organisms but is harder or impossible in thicker tissues or cells from other phyla. Genetically expressed aequorin is easily targeted, but it requires the incorporation of the cofactor coelenterazine to emit light and is very difficult to image because its luminescence produces much less photons than fluorescence. Because aequorin is irreversibly destroyed by  $\text{Ca}^{2+}$  ion, its light output depends on the entire past history of  $\text{Ca}^{2+}$  exposure. To combine the advantages of molecular biological targeting and fluorescence readout, we previously designed fluorescent protein indicators for  $\text{Ca}^{2+}$ , “cameleons” (3). Cameleons are chimeric proteins consisting of a blue or cyan mutant of green fluorescent protein (GFP), calmodulin (CaM), a glycylglycine linker (4), the CaM-binding domain of myosin light chain kinase (M13) (5), and a green or yellow version of GFP.  $\text{Ca}^{2+}$  binding to the CaM causes intramolecular CaM binding to M13. The resulting change from an extended to a more compact conformation increases the efficiency of fluorescence resonance energy transfer between the shorter to the longer wavelength mutant GFP. To obtain adequate expression and brightness of the mutant GFPs in mammalian cells, enhanced genes with mammalian codon usage and mutations for im-

proved folding at 37°C were developed (6). Also the blue mutant proved to be the dimmest and most bleachable of the GFPs. It also required ultraviolet excitation, which is potentially injurious, excites the most cellular autofluorescence, and could interfere with the use of caged compounds. Therefore, we substituted enhanced cyan and yellow fluorescent proteins (ECFP and EYFP) for the original blue and green mutants, respectively (3), to make “yellow cameleons” (YCs). Their affinity for  $\text{Ca}^{2+}$  was tunable by mutations in the  $\text{Ca}^{2+}$  binding loops of CaM (3, 7). Cameleons were targeted to specific intracellular sites by fusing them to appropriate organellar targeting signals or localized host proteins to observe local  $\text{Ca}^{2+}$  dynamics. For example, we engineered two low-affinity indicators, YC3 and YC4, to reside in the lumen of endoplasmic reticulum, where the  $[\text{Ca}^{2+}]$  ranged from 60 to 400  $\mu\text{M}$  at rest, and 1 to 50  $\mu\text{M}$  after agonist-induced mobilization of  $\text{Ca}^{2+}$  (3).

The original YCs had problems such as sensitivity of EYFP to quenching by acidification at pHs close to physiological (8). Such quenching perturbs the signals of YCs, mimicking a decrease in  $[\text{Ca}^{2+}]$ . Furthermore, the incorporation of CaM into the indicator naturally raised concerns that it may interfere with endogenous CaM-stimulated pathways or that it may be perturbed by endogenous CaM or CaM-binding proteins. We have now developed improved YCs that are more resistant to acidification and examined the effects of varying protein expression levels.

### MATERIALS AND METHODS

**In Vitro Protein Characterization.** Relative to wild-type GFP, the significant mutations in the GFP variants are: ECFP, F64L/S65T/Y66W/N146I/M153T/V163A/N164H; EYFP, S65G/S72A/T203Y; and EYFP-V68L/Q69K, S65G/V68L/Q69K/S72A/T203Y. Expression, spectroscopy, and  $\text{Ca}^{2+}$  titrations of recombinant proteins followed previous procedures (3, 9). After elution of the polyhistidine-tagged proteins from nickel-chelate columns, the proteins were concentrated with Centricon 30 filters (Amicon), and were further purified by gel-filtration or ion-exchange chromatography. For pH titrations, a series of buffers were prepared with pHs ranging from 4 to 10.5 in either 50 mM acetate, 2-(*N*-morpholino)ethanesulfonate, 3-(*N*-morpholino)propanesulfonate, Hepes, Tris, or glycine in the presence of 100 mM KCl. The GFP variants were concentrated and buffer-changed into 5 mM Hepes, pH 7.0. The concentrated protein was diluted  $\approx$ 100-fold with the

Abbreviations: GFP, green fluorescent protein; CaM, calmodulin; M13, the CaM-binding domain of myosin light chain kinase; CMV, cytomegalovirus; ECFP, enhanced cyan fluorescent protein; EYFP, enhanced yellow fluorescent protein; PDE, phosphodiesterase; YC, yellow cameleon;  $[\text{Ca}^{2+}]_c$ , cytosolic free  $\text{Ca}^{2+}$  concentration.

<sup>†</sup>Present address: Cell Function & Dynamics, Brain Science Institute, RIKEN, 2-1 Hirosawa, Wako, Saitama 351-0198, Japan.

<sup>§</sup>Present address: Aurora Biosciences Corporation, 11010 Torreyana Road, San Diego, CA 92121.

<sup>¶</sup>To whom reprint requests should be addressed. e-mail: rtsien@ucsd.edu.

The publication costs of this article were defrayed in part by page charge payment. This article must therefore be hereby marked “advertisement” in accordance with 18 U.S.C. §1734 solely to indicate this fact.

PNAS is available online at www.pnas.org.

appropriate buffer to a final concentration of 2  $\mu$ M. The same protein sample was used for absorbance and fluorescence measurements.

**Adenoviral Transfection.** cDNAs coding for YC2 or YC2.1 were cloned into the shuttle plasmid pXCJL under control of the cytomegalovirus (CMV) promoter to generate pXCJL-CMV-YC2 or pXCJL-CMV-YC2.1. These were cotransfected into 293 cells with pJM17, a plasmid containing the entire genome of human adenovirus type 5 (10). Adenoviral vectors AdCMV-YC2 and AdCMV-YC2.1 were generated by homologous recombination and selection of plaques. After two rounds of plaque-purification, purified stocks were prepared. Titters were determined by plaque assay on 293 cells.

Hippocampal neurons were prepared from day 17 Sprague-Dawley rat embryos (11), plated in DMEM/10% fetal bovine serum for 24 h, then transferred to Neurobasal medium (GIBCO) and maintained therein until use. After 6–7 days *in vitro*, hippocampal neurons (50,000 per dish) were infected with  $\approx$ 10 million plaque-forming units of either of the above vectors in 2 ml of medium. Neurons were used for imaging 24 h later.

**Imaging.** Live-cell imaging was performed as described (3). To measure cameleon concentrations in cells, the microscope system was calibrated by assembling three coverslips into a wedge-shaped microchamber in which the thickness increased linearly from 0 to 150  $\mu$ m. The space was filled with a solution containing a certain concentration of YC2.1 at zero  $\text{Ca}^{2+}$  and imaged at the same instrument settings as those used for cells. The fluorescence intensities of ECFP and EYFP-V68L/Q69K were proportional to the thickness of the sample. In a separate experiment using a confocal microscope, we collected a z-series of confocal images of HeLa cells expressing YC2.1, and estimated the cell thickness. For example, the perinuclear region, which gave brightest fluorescence using conventional microscopy was, in most cells, 5  $\mu$ m thick. From the prestimulus intensities of ECFP and EYFP-V68L/Q69K of the perinuclear region in transfected HeLa cells to be imaged, we estimated the concentrations of YCs inside the cells, which could be varied from  $<5$   $\mu$ M to 800  $\mu$ M.

**Activation of Phosphodiesterase (PDE).** The activity of cyclic nucleotide PDE (EC 3.1.4.17) from bovine heart was determined by measuring the release of inorganic phosphate from 3',5'-cAMP, using a colorimetric assay (12). The reaction solution (13) contained 30 mM Hepes, 30 mM imidazole (pH 7.5), 2 mM  $\text{MgCl}_2$ , 0.1% BSA, 0.02646 unit of 5'-nucleotidase (Sigma), 0.00184 unit of PDE (Sigma), 100  $\mu$ M  $\text{CaCl}_2$ , and various concentrations of recombinant proteins. After preincubation of the assay mixture for 5 min at 37°C, the reaction was started by adding cAMP to a final concentration of 1.5 mM. After 10 min at 37°C, 50  $\mu$ l of the mixture was transferred to 800  $\mu$ l of color reagent (malachite green/ammonium molybdate/Triton X-100), followed by the addition of 100  $\mu$ l 34% sodium citrate. After 30 min at room temperature, the amount of inorganic phosphate was determined spectrophotometrically at 660 nm.

## RESULTS

**YC2.1 and YC3.1: Improved YCs.** EYFP (=S65G/S72A/T203Y), the original acceptor within YCs, was highly pH sensitive. Decreasing pH lowered both the absorbance at 511 nm in parallel with the fluorescence (Fig. 1A,  $\bullet$  and  $\circ$ , respectively), both of which were well described by an apparent  $\text{pK}_a$  of 6.9 and a Hill coefficient of 1.0. Therefore, the ratio of 528:476 nm emissions increased not only with increasing  $[\text{Ca}^{2+}]$  but also higher pH within the physiological range. The pH sensitivity (Fig. 1B) was greater at high  $\text{Ca}^{2+}$  (Fig. 1B,  $\bullet$ ) than at zero  $\text{Ca}^{2+}$  (Fig. 1B,  $\circ$ ), as expected because fluorescence resonance energy transfer from the relatively pH-insensitive ECFP (8) to the pH-sensitive EYFP is more

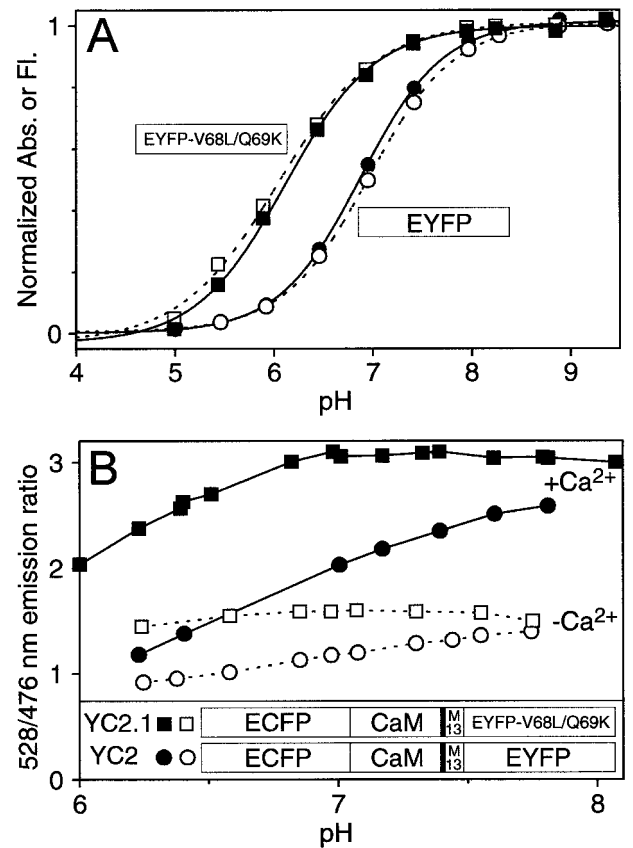


Fig. 1. (A) pH-dependency of normalized amplitudes of 514 nm absorbance ( $\blacksquare$ ,  $\bullet$ ) and 528 nm emission ( $\square$ ,  $\circ$ ; excitation was at 510 nm) of EYFP ( $\circ$ ,  $\bullet$ ) and EYFP-V68L/Q69K ( $\blacksquare$ ,  $\square$ ). EYFP-V68L/Q69K is synonymous with "10C Q69K" (15). During the titrations, no shift in absorbance or emission maximum was observed. (B) pH-dependency of YC2 ( $\bullet$ ,  $\circ$ ) and YC2.1 ( $\blacksquare$ ,  $\square$ ). The emission ratios (528/476 nm) were measured in the presence of 100  $\mu$ M  $\text{CaCl}_2$  ( $\blacksquare$ ,  $\bullet$ ) or 100  $\mu$ M EGTA ( $\square$ ,  $\circ$ ) at various pHs. (Inset) Schematic structures of YC2.1 and YC2.

efficient at high  $\text{Ca}^{2+}$ . The overall pH-sensitivity meant that measurements of cytosolic free  $[\text{Ca}^{2+}]_c$  with such cameleons would require careful checking or clamping of the ambient pH to calibrate the  $\text{Ca}^{2+}$  signal to avoid pH-related artifacts.

The obvious solution was to find a less pH-sensitive version of EYFP, so we tested its existing variants. Adding the mutation Q69K to 10C (S65G, V68L, S72A, T203Y) (14) increases the peak excitation and emission wavelengths by  $\approx$ 2 nm to 516 nm and 529 nm, respectively (15). We have now found that Q69K also drops the apparent  $\text{pK}_a$  to 6.1 (Fig. 1A,  $\blacksquare$  and  $\square$ ), considerably decreasing the sensitivity to pH changes near neutrality. The Hill coefficient (0.9) is hardly changed. Q69 is fairly close to the buried chromophore anion (14), so that mutation to a positively charged lysine could plausibly hinder protonation of the chromophore. 10C Q69K (=EYFP-V68L/Q69K) can be substituted for the original EYFP without altering the YCs'  $\text{Ca}^{2+}$ -dependent fluorescence resonance energy transfer changes, because the two EYFPs have similar fluorescence properties other than pH-sensitivity. YC2 incorporating EYFP-V68L/Q69K was constructed and termed YC2.1; it is much less pH-sensitive (Fig. 1B,  $\blacksquare$  and  $\square$ ) than the original YC2. YC2.1 and the analogous YC3.1 give  $\approx$ 2-fold increase in emission ratio between zero and saturating  $\text{Ca}^{2+}$  (Fig. 2A). Fig. 2B illustrates  $\text{Ca}^{2+}$  titration curves of the emission ratios of YC2.1 and YC3.1 ( $\bullet$  and  $\circ$ , respectively). YC2.1 shows a biphasic  $\text{Ca}^{2+}$  dependency (apparent  $\text{Ca}^{2+}$  dissociation constants  $K'_d$ , 100 nM and 4.3  $\mu$ M;  $n$ , 1.8 and 0.6)

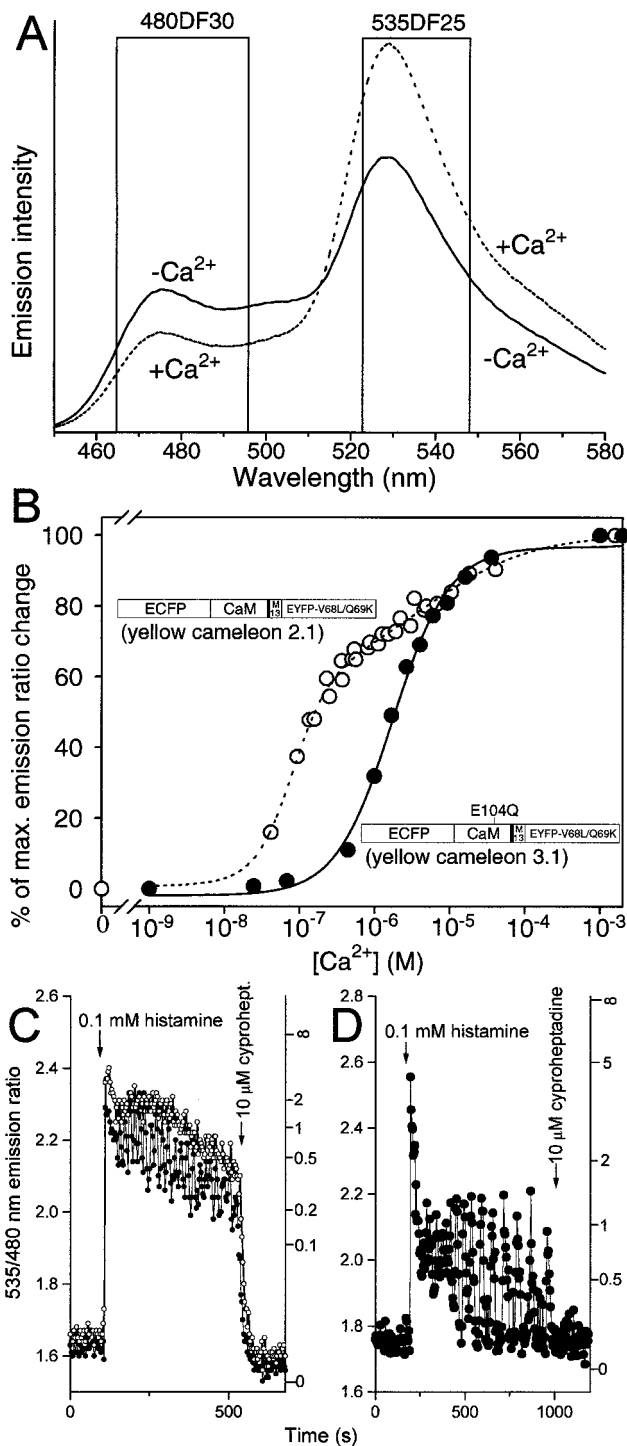


FIG. 2. (A) Emission spectra of YC2.1 (excited at 432 nm) with 100  $\mu\text{M}$  EGTA (solid line) and 100  $\mu\text{M}$   $\text{CaCl}_2$  (dotted line) at pH 7.3. Nominal bandpasses for ECFP (480DF30) and EYFP-V68L/Q69K (535DF25) emission filters are indicated by boxes. (B)  $\text{Ca}^{2+}$  titration curves of YC2.1 ( $\circ$ ) and YC3.1 ( $\bullet$ ), with domain structures of these proteins overlaid. E104Q denotes mutation of the conserved bidentate glutamic acid to glutamine at position 12 of the third  $\text{Ca}^{2+}$ -binding loop of CaM. The data points were from four independent experiments using  $\text{Ca}^{2+}$ /EGTA and  $\text{Ca}^{2+}$ /*N*-(hydroxyethyl)ethylenediamine-*N,N,N'*-triacetate buffer systems (30). The changes in emission ratio (528/476 nm) were normalized to the effects of full  $\text{Ca}^{2+}$  saturation, which were 90–100% increases in ratio over the value at zero  $\text{Ca}^{2+}$ . (C and D) Typical  $\text{Ca}^{2+}$  transients reported by 40–60  $\mu\text{M}$  YC2.1 (C) and YC3.1 (D) in HeLa cells induced by 0.1 mM histamine. A 480  $\pm$  25 nm bandpass filter was used for ECFP emission. The sampling interval was 4–5 sec. The right-hand ordinates calibrate  $[\text{Ca}^{2+}]_c$  in  $\mu\text{M}$ .

and is most responsive near basal cytosolic  $\text{Ca}^{2+}$  concentrations. YC3.1 displays a monophasic  $\text{Ca}^{2+}$  response curve ( $K_d$ , 1.5  $\mu\text{M}$ ;  $n$ , 1.1) and should be helpful in quantifying relatively large  $[\text{Ca}^{2+}]_c$  transients.

To compare the behavior of YC 2.1 with YC 3.1 in live cells, they were separately transfected into HeLa cells. A supra-maximal dose of histamine (0.1 mM) caused an initial peak and subsequent plateau in  $[\text{Ca}^{2+}]_c$  that nearly saturated the YC2.1 response (Fig. 2C), though in one cell a sustained oscillation with a mean frequency of 0.05 Hz was superimposed upon the plateau. Application of cyproheptadine, a histamine antagonist, caused a large fall in  $[\text{Ca}^{2+}]_c$  to previous resting values. By contrast, YC3.1 (Fig. 2D) reported apparently much sharper spikes of  $[\text{Ca}^{2+}]_c$ . All the spikes except for the very first reached only about halfway between  $R_{\min}$  and  $R_{\max}$ , indicating that their amplitude was approximately equal to the  $K_d$  of YC3.1 for  $\text{Ca}^{2+}$ , 1.5  $\mu\text{M}$ . However, the relatively weak  $\text{Ca}^{2+}$  affinity also prevented detection of the sustained plateau elevation between spikes. Therefore, the only apparent effect of cyproheptadine was to stop the oscillations.

Mobilization of  $[\text{Ca}^{2+}]_c$  in HeLa cells by agonists such as histamine did not cause  $\text{pH}_i$  changes detectable by the pH indicator BCECF (data not shown). Correspondingly, comparisons of YC2 vs. YC2.1 and YC3 vs. YC3.1 in HeLa cells showed no differences in reported  $[\text{Ca}^{2+}]_c$  attributable to the different pH sensitivities. However, significant alkalinization and acidification of the cytosol may generally occur during conditions such as mitogenic stimulation and metabolic stress, respectively. Neuronal activity can give rise to significant changes in intracellular and extracellular pH, such as cytosolic acidification during depolarization and repetitive firing (16). Fig. 3 shows how the improved resistance of the V68L/Q69K variants to acidification can be essential. Glutamate stimulation of neurons not only elevates cytosolic  $\text{Ca}^{2+}$  but lowers intracellular pH by  $\approx 0.41$  units (17). YC2 and YC2.1 were expressed in dissociated hippocampal neurons using adenovirus-mediated gene transfer. The labeling extended to the finest processes (Fig. 3A). However, YC2 (Fig. 3B) reported that  $[\text{Ca}^{2+}]_c$  rose only transiently in the sustained presence of 10  $\mu\text{M}$  glutamate, then fell to a level apparently well below the prestimulus baseline. This effect is an artifact of the pH sensitivity of YC2, because YC2.1 indicated a relatively sustained yet reversible  $\text{Ca}^{2+}$  increase (Fig. 3C) as expected.

Although YC 2.1 and YC3.1 are almost indifferent to pH changes from 6.5 to 8, even better acceptor GFPs would still be desirable for the following reasons: (i) Improved YCs are still perturbed by pHs below 6.5. For example, preliminary attempts to observe  $\text{Ca}^{2+}$  in the Golgi lumen have not yet been successful because the  $\text{Ca}^{2+}$  signals are obscured by pH changes (J. Llopis, A.M., and R.Y.T., unpublished results). At pH values below  $\approx 6$ , the pH sensitivities of the ECFP quantum yield and the CaM-M13 interaction might also have to be considered and corrected for. (ii) EYFP-V68L/Q69K seems to fold poorly in the endoplasmic reticulum at 37°C, so expression of YC3.1 in that organelle required shifting the incubation temperature to 30°C for several hours. In mammalian cytosol at 37°C, YC2.1, and YC3.1 were expressed as well as YC2 and YC3. (iii) YFPs can be photobleached by intense illumination at their main absorbance peak. This bleaching is at least partly reversible by illumination at UV and violet wavelengths, showing that it represents photochromism rather than true bleaching (18). In YCs, a slight reduction in yellow/cyan emission ratio was sometimes seen upon increasing the excitation intensity to levels substantially higher than used in the present experiments. This reduction could be largely reversed by delivering a UV prepulse before each measurement, which argues that the artifact was due to photochromism and provides a partial cure. However, a nonphotochromic EYFP would be a more fundamental solution.

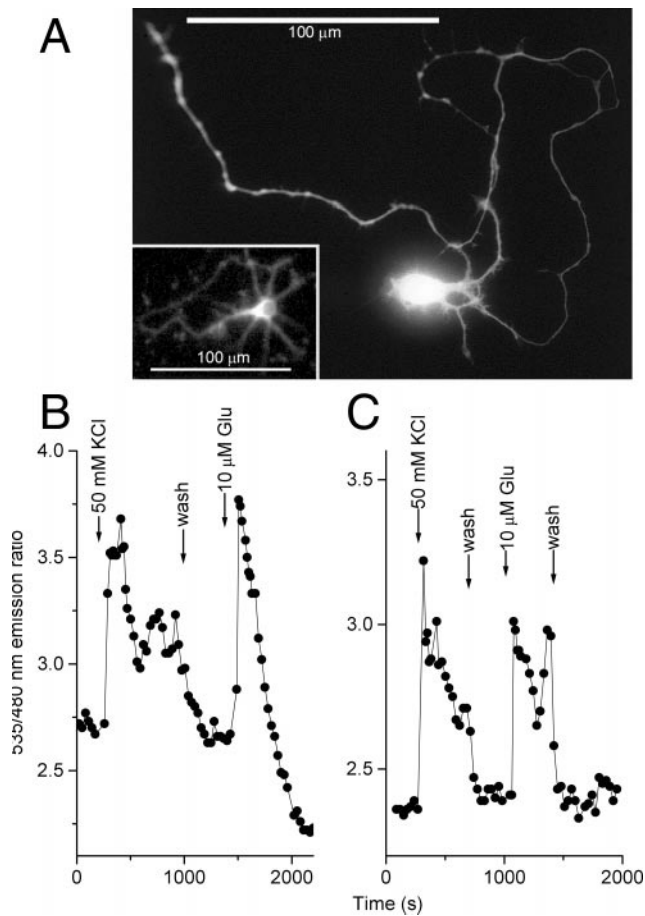


FIG. 3. Measurement of  $[Ca^{2+}]_c$  in hippocampal neurons using YCs. (A) Individual neuron expressing YC2.1 for 24 h, digitized from a photomicrograph. (Inset) The actual cell monitored in C; resolution was reduced by the  $2 \times 2$  binning of the camera. (B and C):  $[Ca^{2+}]_c$  in individual cultured hippocampal neurons (7 days *in vitro*) 24 h after transfection with YC2 (B) or YC2.1 (C). Note the pH artifact in A after stimulation with  $10 \mu\text{M}$  glutamate, resulting in an apparent drop of the emission ratio.

**Concentration of YCs Inside Cells.** Wild-type GFP undergoes changes in its absorption spectrum as a function of protein concentration (19), implying some form of aggregation. To test whether YCs might associate intermolecularly at high concentrations, we measured emission ratios of  $Ca^{2+}$ -free and  $Ca^{2+}$ -saturated YC2.1 at protein concentrations ranging from 0.01 to  $500 \mu\text{M}$  by using a conventional fluorometer at low concentrations and imaging of a microchamber (see *Materials and Methods*) at high concentrations (Fig. 4A). The only variation in ratio was a slight decrease in emission ratio for the  $Ca^{2+}$ -saturated form at concentrations above  $300 \mu\text{M}$ . If the ECFP within one molecule of YC had a tendency to bind to the EYFP from another YC, the emission ratio should increase with YC concentration in the absence of  $Ca^{2+}$ , but little or no such trend is seen.

We investigated the ability of various concentrations of YC3.1 to buffer  $Ca^{2+}$  transients in HeLa cells. Fig. 4B compares the  $[Ca^{2+}]_c$  response with  $0.1 \text{ mM}$  histamine administered with three neighboring cells expressing different levels of YC3.1 (*a* and *b*,  $150 \mu\text{M}$ ; *c*,  $500 \mu\text{M}$ ). Sharp  $[Ca^{2+}]_c$  transients followed by  $[Ca^{2+}]_c$  oscillations were observed in cells *a* and *b*. In contrast,  $[Ca^{2+}]_c$  in cell *c* recovered slowly to the baseline over a period of several hundred seconds. Oscillations were never observed with  $>300 \mu\text{M}$  of YC3.1 in transfected HeLa cells. Because each cameleon can bind four  $Ca^{2+}$ , it is not surprising that the introduction of millimolar concentrations of

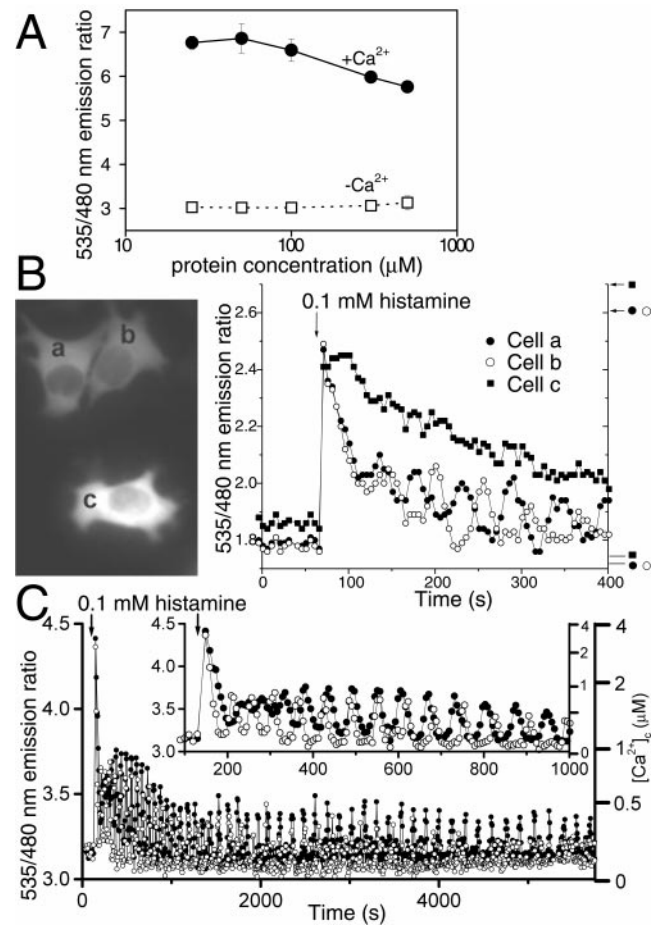


FIG. 4. (A) Concentration effects on emission ratios of YC2.1 in a cuvette at pH 7.3 in the presence of  $100 \mu\text{M}$   $CaCl_2$  (●) and  $100 \mu\text{M}$  EGTA (□). Each data point represents the mean of 10–15 determinations. (B) The effects of two different concentrations of YC3.1 on histamine-induced  $Ca^{2+}$  transients in HeLa cells. Indicator concentrations were estimated to be  $150 \mu\text{M}$  in cells *a* and *b* and  $500 \mu\text{M}$  in cell *c*. (Left) Fluorescence images of the three cells. (Right) Time courses of emission ratios from cells *a* (●), *b* (○), and *c* (■). The arrows and horizontal bars on the right indicate  $R_{max}$  and  $R_{min}$ , respectively. (C) Oscillations in  $[Ca^{2+}]_c$  induced by  $0.1 \text{ mM}$  histamine in two HeLa cells expressing  $40 \mu\text{M}$  YC3.1. ECFP emission was read with a  $480 \pm 15 \text{ nm}$  filter. (Inset) The initial response on an expanded time scale.

$Ca^{2+}$  binding sites would significantly buffer  $[Ca^{2+}]_c$  dynamics. A controlled ability to increase indicator concentrations to levels that significantly buffer  $[Ca^{2+}]_c$  can be very useful, for example to measure total fluxes of  $Ca^{2+}$  (20) and to test whether  $[Ca^{2+}]_c$  changes are necessary for physiological responses.

Fig. 4C shows a typical pattern of histamine-stimulated  $[Ca^{2+}]_c$  oscillations reported by  $\approx 40 \mu\text{M}$  YC3.1 in two HeLa cells. The asynchronized responses each began with a large spike exceeding  $2 \mu\text{M}$ , became sinusoidal, then converted into spikes of up to  $0.5 \mu\text{M}$  and gradually declining frequency. The later spikes were preceded by slow pacemaker increases (21). This record illustrates some advantages of YCs over previous indicators even in simple tissue culture: emission ratiometric readout in single cells, easy calibration up to several  $\mu\text{M}$   $[Ca^{2+}]_c$ , and practically unlimited recording times with no indicator leakage, compartmentation, exhaustion, or cumulative photodestruction.

How low can cameleon concentrations be lowered? Cytosolic concentrations below  $20 \mu\text{M}$  were generally too dim to give good signal to noise ratios in dynamic single-cell imaging. Increasing the intensity of illumination could not compensate

because of EYFP photochromism. We established stable mammalian cell lines constitutively expressing YC2.1 and YC3.1, which proliferated at normal rates. In both lines, the indicators were uniformly distributed in the cytosol but excluded from the nucleus, and  $[Ca^{2+}]_c$  transients were similar to those in transiently transfected cells (data not shown). The maintained exclusion from the nucleus and  $[Ca^{2+}]_c$  sensitivity argued that the indicator proteins remain stable and unproteolyzed, because cleavage between the CaM and M13 would generate split cameleon, whose components are small enough to enter the nucleus, and cleavage anywhere else would destroy  $[Ca^{2+}]_c$ -dependent fluorescence resonance energy transfer.

**Interaction with CaM and CaM-Dependent Enzymes.** Because CaM interacts with so many targets inside cells, one might be concerned about interaction between intact or split cameleons and endogenous CaM or CaM binding proteins. For example, overexpression of CaM without a binding partner accelerates the rate of growth of cultured cells (22) and cardiomyocytes in transgenic mice (23). We compared *in vitro* the ability of recombinant CaM, YC2.1, YC3.1, and split YC2.1 (equimolar ECFP-CaM and M13-EYFP-V68L/Q69K) to stimulate a prototypical CaM-dependent enzyme, PDE. We measured PDE activity colorimetrically (13) at saturating  $[Ca^{2+}]$  (100  $\mu$ M) as a function of activator protein concentration (Fig. 5A). 8 nM CaM gave half-maximal PDE activity. ECFP-CaM gave the same  $EC_{50}$  value (data not shown). The dose-response curve for split YC2.1 was shifted rightward ( $EC_{50}$  45 nM), indicating that M13-EYFP-V68L/Q69K competed with PDE for ECFP-CaM. However, PDE was barely activated by YC2.1 ( $EC_{50}$ , 1.5  $\mu$ M) and YC3.1 ( $EC_{50}$ , 4.0  $\mu$ M). These  $EC_{50}$ s are 2 to 3 orders of magnitude greater than those of the split constructs. Conceivably they could result from  $\approx 1\%$  proteolysis of the fusion, in which case the true  $EC_{50}$ s for the intact cameleons could be even higher. Assuming that the spatially-averaged concentration of native CaM inside cells is from 10 to 100  $\mu$ M (24, 25), then as much as 1 mM YCs should not unduly disturb the  $Ca^{2+}$  and CaM dependent cascades that occur naturally. Therefore, the primary effect of excessive cameleon concentrations is likely to be simple buffering of  $[Ca^{2+}]_c$  rather than interference with CaM-mediated signaling.

The converse question was the extent to which the emission ratio signals of intact or split YCs were perturbed by excess CaM. We were more concerned about perturbation of YC3.1, because the E104Q mutation in its CaM sacrificed the high  $Ca^{2+}$  affinity component of the response. Native CaM might compete with the internal CaM-E104Q for the M13 peptide, especially at low but nonzero  $[Ca^{2+}]$ . Fig. 5B shows  $Ca^{2+}$  titration curves of YC3.1 in the absence and presence of a ten-fold excess of CaM, which did not significantly perturb either the dynamic range of the  $Ca^{2+}$ -dependent emission ratio change (from 1.3 to 2.0) or the  $Ca^{2+}$  dependency. We verified such resistance to CaM also for YC2.1. In contrast, the response of split YC2.1 (1  $\mu$ M) to  $Ca^{2+}$  was severely perturbed by CaM as expected (Fig. 5C). An equal concentration of CaM (1  $\mu$ M) reduced the  $Ca^{2+}$  dependent emission ratio change by  $\approx 50\%$ . An 8-fold excess of CaM (8  $\mu$ M) almost completely eliminated the  $Ca^{2+}$ -dependent change in ratio.

These *in vitro* data demonstrate that the fused CaM and M13 in YCs preferentially interact with each other upon  $Ca^{2+}$  elevation rather than with separate molecules of CaM or CaM-binding proteins. When the CaM and M13 are left separate as in the split cameleons, they are fully subject to cross-reaction with unlabeled CaM and presumably CaM partners. This comparison exemplifies the ability of forced proximity to channel the interactions of proteins or their domains. Interestingly, fusion of two GFPs to opposite ends of a CaM target peptide, equivalent to omitting CaM from a cameleon, produces a complementary class of indicators that are specifically sensitive to endogenous  $(Ca^{2+})_c$ -CaM (26).

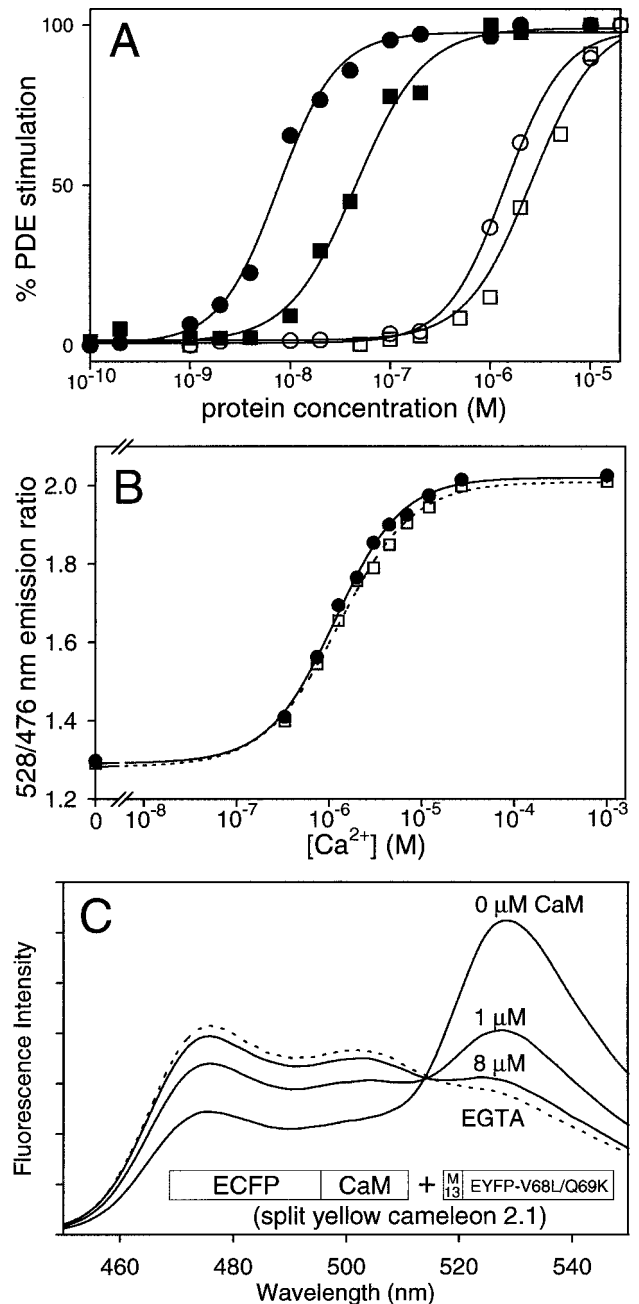


Fig. 5. Interaction of intact and split cameleons with PDE and CaM. (A) The relative level of PDE stimulation is shown as a function of the concentration of recombinant CaM (●), split YC2.1 (■), YC2.1 (○), and YC3.1 (□). (B)  $Ca^{2+}$  dependency of YC3.1 (0.3  $\mu$ M) in the absence (■) and presence (□) of excess CaM (3  $\mu$ M). The titrations were done by using a  $Ca^{2+}$ /N-(hydroxyethyl)ethylenediamine-N,N',N'-triacetate buffer system (30) at pH 7.1 (C) Emission spectra of split YC2.1 (1  $\mu$ M) with 100  $\mu$ M EGTA (dotted line), and with 1 mM  $CaCl_2$  (solid lines) when preincubated with 0, 1, and 8  $\mu$ M CaM. Also shown is the schematic structure of split YC2.1, the equimolar mixture of ECFP-CaM and M13-EYFP-V68L/Q69K.

As further evidence against major interaction between YCs and endogenous CaM in cells, the dynamic range of the  $Ca^{2+}$ -dependent emission ratio change of YCs in HeLa cells is 1.6–2.0, which is similar to that obtained by using the same microscope for recombinant YCs in a simple solution (1.8–2.2). On the other hand, split YCs are greatly perturbed by CaM. Although they exhibit a 4-fold emission ratio change *in vitro*, the ratio of  $R_{max}$  to  $R_{min}$  in HeLa cells has been at most 2.5-fold. This diminution likely depends upon the molar ratios

of ECFP-CaM, M13-EYFP, and native CaM. Also, increases in  $[Ca^{2+}]_c$  often cause migration of CaM, but YCs always remain uniformly distributed in cytosol. By contrast, ECFP-CaM and M13-EYFP-V68L/Q69K often were unevenly distributed between nucleus and cytosol (results not shown), which sometimes changed during  $[Ca^{2+}]_c$  increases, again indicating that split cameleons do interact with endogenous proteins to a much greater extent. Split cameleons are significant not as routine indicators of  $[Ca^{2+}]_c$  but rather as a prototype example of the nondestructive detection and imaging of dynamically modulated protein-protein heterodimerization, a much more general challenge in cell biology and biochemistry.

## DISCUSSION

In this study, we have considerably decreased the pH-sensitivity of YCs, quantified the intracellular indicator concentrations, assessed what concentrations cause major buffering of  $[Ca^{2+}]_c$ , and shown that YCs interact very little with CaM and CaM target proteins. Full exploitation of cameleons as genetically encoded  $Ca^{2+}$  indicators requires efficient means for getting the genes into a wide variety of tissues including differentiated, postmitotic cells. Three methods that are proving successful are, in increasing order of laboriousness: (i) In ballistic particle-mediated gene transfer (Biolistics, BioRad), the cDNA molecules are adsorbed to gold particles, which are shot by a high-pressure gas jet into the tissue or culture. No genetic engineering is required, but only a small and random fraction of the cells end up expressing the gene. (ii) Recombinant adenoviruses have proved to be efficient, noncytotoxic for transfecting neurons in dissociated (Fig. 3) and organotypic cultures (results not shown), as well as primary cultures from other organs such as liver. Because adenovirus vectors can deliver exogenous genes of up to several kilobases (10), the introduction of YC genes ( $\approx 2$  kb) is not a problem. (iii) Transgenic nematodes (27) and mice expressing the YCs have been produced. In the nematodes, the cameleons have been targeted to specific cell types by appropriate tissue-specific promoters, and video-rate image sequences of  $[Ca^{2+}]_c$  fluctuations *in vivo* have been obtained by high-speed two-photon-excitation microscopy (27). In mice, the use of the tissue-nonspecific  $\beta$ -actin promoters has given expression in a mosaic of cells in nearly all tissues (D. Zacharias, V. Lev-Ram, and R.Y.T., unpublished results). These animals are undergoing further analysis. The ability of two-photon excitation microscopy to excite and recover signals originating inside scattering tissue (28) should be even more valuable in the transgenic mice. Thus the cameleons and two-photon excitation are complementary: the cameleons provide genetic means to implant functional indicators deep inside a tissue or organism, and multiphoton microscopy retrieves their fluorescence signals while minimizing photochromic effects (29).

We thank S. R. Adams, A. Cubitt, J. Llopis, and D. Zacharias for helpful discussion. This work was supported by Howard Hughes Medical Institute, National Institute of Neurological Disorders and Stroke (NS27177 to R.Y.T.), and a Human Frontier Science Program long-term fellowship to A.M.

1. Tsien, R. Y. (1989) *Annu. Rev. Neurosci.* **12**, 227–253.
2. Brini, M., Marsault, R., Bastianutto, C., Alvarez, J., Pozzan, T. & Rizzuto, R. (1995) *J. Biol. Chem.* **270**, 9896–9903.
3. Miyawaki, A., Llopis, J., Heim, R., McCaffery, J. M., Adams, J. A., Ikura, M. & Tsien, R. Y. (1997) *Nature (London)* **388**, 882–887.
4. Porumb, T., Yau, P., Harvey, T. S. & Ikura, M. (1994) *Protein Eng.* **7**, 109–115.
5. Ikura, M., Clore, G. M., Gronenborn, A. M., Zhu, G., Klee, C. B. & Bax, A. (1992) *Science* **256**, 632–638.
6. Zolotukhin, S., Potter, M., Hauswirth, W., Guy, J. & Muzyczka, N. (1996) *J. Virol.* **70**, 4646–4654.
7. Gao, Z. H., Krebs, J., VanBerkum, M. F. A., Tang, W. J., Maune, J. F., Means, A. R., Stull, J. T. & Beckingham, K. (1993) *J. Biol. Chem.* **268**, 20096–20104.
8. Llopis, J., McCaffery, J. M., Miyawaki, A., Farquhar, M. G. & Tsien, R. Y. (1998) *Proc. Natl. Acad. Sci. USA* **95**, 6803–6808.
9. Heim, R. & Tsien, R. Y. (1996) *Curr. Biol.* **6**, 178–182.
10. Graham, F. L. & Prevec, L. (1991) *Methods Mol. Biol.* **7**, 109–128.
11. Zafra, F., Hengerer, B., Leibrock, J., Thoenen, H. & Lindholm, D. (1990) *EMBO J.* **9**, 3545–3550.
12. Lanzetta, P. A., Alvarez, L. J., Reinach, P. S. & Candia, O. A. (1979) *Anal. Biochem.* **100**, 95–97.
13. Rhyner, J. A., Koller, M., Durussel-Gerber, I., Cox, J. A. & Strehler, E. E. (1992) *Biochemistry* **31**, 12826–12832.
14. Orm6, M., Cubitt, A. B., Kallio, K., Gross, L. A., Tsien, R. Y. & Remington, S. J. (1996) *Science* **273**, 1392–1395.
15. Tsien, R. Y. (1998) *Annu. Rev. Biochem.* **67**, 509–544.
16. Chesler, M. & Kaila, K. (1992) *Trends Neurosci.* **15**, 396–402.
17. Wang, G. J., Randall, R. D. & Thayer, S. A. (1994) *J. Neurophysiol.* **6**, 2563–2569.
18. Dickson, R. M., Cubitt, A. B., Tsien, R. Y. & Moerner, W. E. (1997) *Nature (London)* **388**, 355–358.
19. Ward, W. W., Prentice, H. J., Roth, A. F., Cody, C. W. & Reeves, S. C. (1982) *Photochem. Photobiol.* **35**, 803–808.
20. Schneggenburger, R., Zhou, Z., Konnerth, A. & Neher, E. (1993) *Neuron* **11**, 133–143.
21. Bootman, M. D. & Berridge, M. J. (1996) *Curr. Biol.* **6**, 855–865.
22. Ramussen, C. D. & Means, A. R. (1987) *EMBO J.* **6**, 3961–3968.
23. Gruver, C. L., Francesco, D., Goldstein, M. A. & Means, A. R. (1993) *Endocrinology* **133**, 376–388.
24. Cartaud, A., Ozon, R., Walsh, M. P., Haiech, J. & Demaille, J. G. (1980) *J. Biol. Chem.* **255**, 9404–9408.
25. Kakiuchi, S., Yasuda, S., Yamazaki, R., Teshima, Y., Kanda, K., Kakiuchi, R. & Sobue, K. (1982) *J. Biochem.* **92**, 1041–1048.
26. Romoser, V. A., Hinkle, P. M. & Persechini, A. (1997) *J. Biol. Chem.* **272**, 13270–13274.
27. Kerr, R. A., Baird, G., Schafer, W. R. & Tsien, R. Y. (1998) *Abstracts of the Fifth International Congress of Neuroethology*, S4.
28. Denk, W. & Svoboda, K. (1997) *Neuron* **18**, 351–357.
29. Fan, G. Y., Fujisaki, H., Miyawaki, A., Tsay, R.-K., Tsien, R. Y. & Ellisman, M. H. (1999) *Biophys. J.*, in press.
30. Tsien, R. Y. & Pozzan, T. (1989) *Methods Enzymol.* **172**, 230–262.